

## Article

# Identifying the Spatio-Temporal Change in Winter Wheat–Summer Maize Planting Structure in the North China Plain between 2001 and 2020

Bo Yang <sup>1,2</sup>, Jinglei Wang <sup>1</sup>, Shenglin Li <sup>1,2</sup> and Xiuqiao Huang <sup>1,\*</sup>

<sup>1</sup> Farmland Irrigation Research Institute, Chinese Academy of Agricultural Sciences, Xinxiang 453002, China; yangbo01@caas.cn (B.Y.); wangjinglei@caas.cn (J.W.); 82101221064@caas.cn (S.L.)

<sup>2</sup> Graduate School of Chinese Academy of Agricultural Sciences, Beijing 100081, China

\* Correspondence: huangxiuqiao@caas.cn

**Abstract:** Tracking winter wheat–summer maize distribution is crucial for the management of agricultural water resources in the water-scarce North China Plain (NCP). However, the spatio-temporal change in planting structure that has occurred during the last 20 years remains unclear. Therefore, winter wheat–summer maize distribution between 2001 and 2020 was determined via the maximum likelihood algorithm of supervised classification and a threshold method using the MODIS NDVI product MOD13Q1 and Landsat 5/7 images. The results reveal that dividing distributions into six sample categories—winter wheat–summer maize, winter wheat–rice, spring maize, cotton, other double-cropping systems, and fruit trees—proved to be an efficient way to discriminate winter wheat–summer maize distribution, with  $R^2$  and RMSE values ranging from 0.738 to 0.901 and from 179.05 to 215.72 km<sup>2</sup>, respectively. From 2001 to 2020, the planting area continually expanded, experiencing a significant growth of  $3.32 \times 10^4$  km<sup>2</sup> (23.44%). Specifically, the planting area decreased by 2982.13 km<sup>2</sup> (10.06%) in the northern part of the NCP, including the Beijing–Tianjin–Hebei region, while it increased by  $3.62 \times 10^4$  km<sup>2</sup> (32.30%) in the middle and southern parts, encompassing Shandong, Henan, Anhui, and Jiangsu provinces. The stable growing region was primarily concentrated in the middle of the Hebei Plain, along the Yellow River irrigation areas and humid zones of the southwest, accounting for 75–85% of the total NCP planting area. Our results can provide references for adjusting agricultural planting structures, formulating food security strategies, and optimizing the management of water resources in the NCP.

**Keywords:** MODIS data; Landsat images; winter wheat–summer maize; supervised classification; North China Plain



**Citation:** Yang, B.; Wang, J.; Li, S.; Huang, X. Identifying the Spatio-Temporal Change in Winter Wheat–Summer Maize Planting Structure in the North China Plain between 2001 and 2020. *Agronomy* **2023**, *13*, 2712. <https://doi.org/10.3390/agronomy13112712>

Academic Editors: Dan Li, Yingying Dong and Qiong Zheng

Received: 19 September 2023

Revised: 15 October 2023

Accepted: 25 October 2023

Published: 27 October 2023



**Copyright:** © 2023 by the authors. Licensee MDPI, Basel, Switzerland. This article is an open access article distributed under the terms and conditions of the Creative Commons Attribution (CC BY) license (<https://creativecommons.org/licenses/by/4.0/>).

## 1. Introduction

The North China Plain (NCP) is a major food-producing area in China [1–4], contributing to the production of about 75% and 35% of China’s wheat and maize, respectively [5–7]. The winter wheat and summer maize rotation system is the predominant farming pattern in this area [8]. This dominant cultivation system requires 700–1000 mm yr<sup>−1</sup> water, greatly exceeding the annual average precipitation of 500–600 mm [9], 70% to 80% of which falls during the summer maize growing season, from June to September [10,11]. Precipitation throughout the growing phase of winter wheat is significantly lower than the actual water demand [12], and approximately 70% of the water demand depends on groundwater irrigation [13]. However, continuous groundwater pumping for agricultural production has resulted in a significant reduction in the groundwater table, and this is considered to be the main cause of groundwater over-exploitation in the North China Plain during the course of the last four decades [6,14]. Accurate mapping of winter wheat–summer maize cultivation area in the NCP since 2001 proved fundamental for assessing changes in crop water consumption, thus providing the scientific basis for formulating policies such as

the optimal management of water resources, the sustainable utilization of groundwater resources, and national food security [5,6].

Data on the planting area of winter wheat and summer maize were mainly obtained through two methods: investigation statistics and remote sensing monitoring [15,16]. However, the former method has major problems, such as large errors, time and labor consumption, and the absence of spatial distribution information [17]. Remote sensing has numerous benefits, including the provision of efficient, objective, and consistent data. It is also cheap or even free, which makes it an effective tool for identifying crops at different spatio-temporal scales [5,6,18,19]. However, the extensive and prolonged remote sensing mapping of winter wheat and summer maize in the NCP is still difficult due to the largely dispersed patterns of smallholder farming. The temporal resolution of the Landsat TM/ETM+ satellite is 16 days, and its spatial resolution is 30 m. Despite its high spatial resolution, image quality is often compromised by frequent cloud and aerosol pollution, resulting in fewer valid images [20,21]. Due to its constraints of low temporal resolution and inadequate data quality, Landsat is suitable for field-scale applications, and it is limited to the application of tracking prolonged continuous changes in the NCP crop distribution. MODIS data offer several advantages, including a short revisit period, wide coverage, and the ability to determine phenological characteristics [22–24]. As a result, MODIS has become a major source of remote sensing data for monitoring planting areas in large regions worldwide [25,26].

The normalized difference vegetation index (NDVI) is an extensively utilized index to acquire crop information and is widely used in crop classification and growth evaluation [27,28]. MODIS NDVI products, such as 8-day 0.0025° MOD09Q1 and 16-day 0.0025° MOD13Q1, are commonly utilized. Despite the former having a higher temporal resolution, the latter notably enhances classification accuracy due to its superior data quality [5]. Regarding classification methods, supervised classification using MODIS data is the most commonly employed and effective approach for crop classification [28–30]. The categorization results are influenced by two primary factors: the sample category and the remote-sensing product. Previous studies have shown apparent differences in sample categories, which may result in significant uncertainties [5]. In the NCP, sample categories for classification varied from as few as four (including winter wheat–summer maize, winter wheat–cotton, spring maize, and cotton) [31] to as many as seven (encompassing winter wheat–summer maize, spring maize, cotton, forest, fruit, vegetables, and rice) [32]. Other categories were adopted to capture the complexity of crop and land cover types in the region [33,34]. Combining MODIS and Landsat data can enhance crop identification accuracy [6,27,35]. VI (vegetation index) products with a 250 m spatial resolution can more accurately identify winter wheat–summer maize than those with a 500 m spatial resolution [5].

As a typical double-cropping system in northern Jiangsu, the phenological period of winter wheat–rice is close to that of winter wheat–summer maize, but the former was generally not determined in previous studies, which may affect the classification accuracy of winter wheat–summer maize to some extent. Simultaneously, owing to the bimodal signal of NDVI curves created by the mixed planting system in the NCP, the classification of winter wheat–summer maize is substantially disrupted. However, previous studies typically did not differentiate between these two categories. In addition, earlier studies primarily focused on monitoring winter wheat and summer maize distribution within a single year [3,31,36–38] or analyzing variations in specific regions of the NCP [2,6,33]. The stability of the research methods or models used in these studies remains uncertain, and they often fail to provide dynamic spatio-temporal information on winter wheat–summer maize. In light of this, this study aims to achieve the following objectives: (1) develop an effective method for mapping the distribution of winter wheat–summer maize in the NCP using the maximum likelihood algorithm; (2) evaluate the spatio-temporal change in winter wheat–summer maize distribution for the years 2001, 2010, and 2020.



## 2.2. Dataset

Table 2 shows the sources of the data used in this study. These include MODIS NDVI files (570 images), GlobeLand30 land cover maps, Landsat images, field survey sites, and statistical data. The MOD13Q1 datasets (Terra Vegetation Indices 16-Day L3 Global 250 m SIN Grid V006) corresponding to the strip numbers H26V06, H26V07, H27V06, and H27V07 for 2001, 2010, and 2020 were acquired from NASA's official website [42].

**Table 2.** A summary of this study's data.

Data Name	Temporal Resolution	Spatial Resolution	Time	Acquisition Source
MOD13Q1	16-day	250 m	2001, 2010, 2020	<a href="https://www.earthdata.nasa.gov/">https://www.earthdata.nasa.gov/</a> accessed on 8 June 2021
Landsat 5/7 images	16-day	30 m	2001, 2010, 2020	<a href="https://earthexplorer.usgs.gov/">https://earthexplorer.usgs.gov/</a> accessed on 14 September 2021
GlobeLand30	annual	30 m	2000, 2010, 2020	<a href="http://www.globallandcover.com">www.globallandcover.com</a> accessed on 5 May 2021
Statistic data	annual	county	2001, 2010, 2020	<a href="http://www.stats.gov.cn/sj/">http://www.stats.gov.cn/sj/</a> accessed on 12 April 2022
Field survey sites	one time	in situ	10 September 2020–8 October 2020	Field survey

The Landsat 5TM Collection 2 (C2) Level 1 (L1) and Landsat 7ETM+ Collection 2 (C2) Level 1 (L1) images from 2001, 2010, and 2020 were collected, as shown in Table 3. The path number for Julu County is 123 or 124, with a row number of 34. For Huaiyin District, the path number is 120, and the row number is 37. Landsat NDVI data were computed using surface reflectance bands 3 (red) and 4 (near-infrared) according to the following formula [43]:

$$NDVI = \frac{\rho_{NIR} - \rho_{RED}}{\rho_{NIR} + \rho_{RED}} \quad (1)$$

where  $\rho_{NIR}$  and  $\rho_{RED}$  represent the surface reflection values of the near-infrared band (841–876 nm) and the red band (620–670 nm), respectively.

**Table 3.** General information about Landsat 5/7 images.

Region	Sensor	Date	Cloud Cover/%
Region of 123-034	Landsat-5TM	16 April 2001	0
	Landsat-5TM	2 April 2010	0
Region of 124-034	Landsat-5TM	23 September 2001	6
	Landsat-5TM	2 October 2010	12
	Landsat-7ETM+	28 April 2020	0
	Landsat-7ETM+	19 September 2020	0
Region of 120-037	Landsat-5TM	4 April 2001	1
	Landsat-5TM	27 September 2001	1
	Landsat-5TM	29 April 2010	2
	Landsat-5TM	6 October 2010	11
	Landsat-7ETM+	23 April 2020	1
	Landsat-7ETM+	7 September 2020	0

The GlobeLand30 product was developed by the National Geographic Information Center based on the “Pixel-Object-Knowledge (POK)” approach. More than 130 nations' scientists and users utilize it for modeling surface processes, monitoring geographic conditions, managing urban and rural areas, and analyzing environmental change [44]. Between 10 September and 8 October 2020, field surveys were conducted in the NCP using hand-held GPS devices, and survey routes were strategically planned to encompass the predominant

cropping systems within this region (Figure 1b). Continuous planting areas obviously larger than 250 m × 250 m were chosen as the sample sites. The sum of 1184 field survey sites was gathered, which included 492 winter wheat–summer maize sites, 106 cotton sites, 121 spring maize sites, 253 winter wheat–rice sites, 118 other double-cropping sites (e.g., winter wheat–cotton, winter wheat–soybean, and winter wheat–peanut), and 94 fruit tree sites (e.g., peach and pear). Statistical datasets pertaining to the cultivation area of winter wheat and summer maize in 2001, 2010, and 2020 were sourced from both national and provincial/municipal statistical yearbooks.

### 2.3. Methods

A proposed methodology for accurately identifying major crops in the NCP is presented, including the following procedures. (1) The MOD13Q1 datasets were preprocessed, followed by smoothing the NDVI curves using Savitzky–Golay filtering to generate the fundamental map for categorization. (2) Landsat TM/ETM+ images were used to identify the distribution of winter wheat–summer maize and winter wheat–rice in Julu County and Huaiyin District through the application of the threshold method. (3) The Landsat classification map was integrated to enrich and eliminate the sample sites, resulting in the acquisition of the final classification training and validation sample sites. (4) Three schemes were developed, each consisting of distinct categories. The maximum likelihood classification approach was adopted to identify the distributions of winter wheat and summer maize for the years 2001, 2010, and 2020. (5) The evaluation of the accuracy of the findings was conducted at three different levels: pixel, county, and regional.

#### Data Processing

The composite MOD13Q1 images, spanning a period of 16 days, were mosaicked and reprojected to the Albers projection using the MODIS Reprojection Tool (MRT) and converted, clipped, and synthesized using ENVI 5.3 software. Images of GlobeLand30 were mosaicked, resampled to 250 m, reprojected to the Albers projection, and clipped, then used as the cultivated land mask to extract the crop classification. The NDVI time series curves were reconstructed using Savitzky–Golay filtering with filter parameters set to N Left = 5, N Right = 5, Order = 0, and Degree = 2 to remove noise from the NDVI data.

The Landsat 7 ETM+ sensor's scan-line corrector (SLC) malfunctioned in 2003, leaving around 22% of the pixels in each picture unscanned [45]. Therefore, strip repairs were first performed on the four Landsat 7 images using the ENVI 5.3 Landsat gap-fill tool. Processing of Landsat images included radiation calibration, atmospheric correction, cloud removal processing, NDVI calculation, and NDVI time series synthesis.

### 2.4. Supervised Classification Based on MODIS Data

#### 2.4.1. The Savitzky–Golay Filtering Method

In theory, the curve of NDVI is expected to exhibit continuity and smoothness, mostly attributed to the gradual changes in the canopy cover within a certain timeframe [46]. However, due to cloud interruptions, data transmission errors, bio-directional effects, or the presence of ice and snow cover, abrupt fluctuations invariably occur in certain data points [47]. Maximum composite and cloud detection methods are commonly used in the processing of NDVI temporal datasets, but the residual noise of the datasets can hinder subsequent analyses and lead to erroneous results [48]. The crucial foundation for extracting the phenological features of crops from a multi-temporal NDVI dataset lies in the smoothing and reconstruction of the data sequence. This process aims to minimize noise and reduce data gaps, thereby enhancing the dataset's comparability both inter-annually and regionally [2]. At present, the commonly used noise removal filtering methods include the Savitzky–Golay (S-G) filtering method, double logic blending function filtering (D-L), asymmetric Gaussian filtering (A-G), and Fourier harmonics (HANTS) [49]. Liu et al. [50] conducted a comparative analysis of these four filtering methods using Environmental Satellite NDVI data and concluded that the S-G algorithm was superior to the other three

algorithms and could more clearly reconstruct the detailed changes in the curve and better reflect real-life conditions.

In this paper, the S-G filtering method was used to reconstruct the MODIS NDVI time series image. The S-G method, proposed by Savitzky and Golay, is a filtering method based on local polynomial least square fitting in the time domain. By selecting a certain number of adjacent values near a certain point, the least square method is used to fit an  $n$ -order polynomial, which is then applied to determine the smoothing value of the point [51]. The formula may be expressed as follows:

$$I'_i = \frac{\sum_{j=-n}^n C_j N_{i+j}}{N} \quad (2)$$

where  $I$  represents the original NDVI value;  $I'_i$  represents the fitting NDVI value;  $C_j$  represents the filtering coefficient of the  $j$ th NDVI value;  $N = 2n + 1$  represents the size of the sliding window, which is also the number of convolutions;  $i$  refers to the  $i$ th data; and  $n$  represents half the size of the smooth window.

#### 2.4.2. Classification Method and Sample Selection

Among traditional supervised classification methods, the maximum likelihood classification algorithm is highly prevalent and is commonly regarded by many authors as the standard algorithm [5,29,52]. The study conducted by Arvor et al. [53] revealed that the use of the maximum likelihood classification approach on MOD13Q1 datasets yielded superior crop classification outcomes when compared to the spectral angle mapper classifier and decision tree. The core idea of this approach entails the computation of the likelihood that a pixel belongs to each pre-defined category, followed by the assignment of the pixel to the category with the greatest probability [54]. The field investigation sites were enhanced to acquire a sufficient number of valid sample points, and invalid points were systematically excluded according to certain rules. It should be noted that, from 2001 to 2020, crop types in the NCP remained consistent. However, it was challenging to ensure that the crop type at each field survey site in 2001 and 2010 exactly matched that in 2020. This is attributed to annual variations in planting systems influenced by factors such as market prices, irrigation sources, labor costs, and more [5]. We enhanced the classification sample dataset by removing invalid or erroneous sample points. This process employed three approaches:

- (1) Large fields that surrounded each field survey site in Google Earth were identified as newly added samples. These fields had sizes that were more than  $250 \text{ m} \times 250 \text{ m}$ , and the picture patterns at this site, such as color and texture, were the same as those at the other site [5].
- (2) In the classification results achieved through the Landsat threshold method, winter wheat–summer maize and winter wheat–rice growing areas larger than  $250 \text{ m} \times 250 \text{ m}$  were selected as new samples for MODIS supervised classification. The threshold method is actually a decision tree method that completes the classification by setting the NDVI threshold in the critical period of different crop phenology.
- (3) The NDVI time series curves of all samples from 2001 to 2020 were extracted, and unsuitable sample points were screened. Since different planting types have unique NDVI timing curves, the screening rules include two sections. (1) The NDVI curve features of each sample site should correspond to their respective planting types and have a unique phenological calendar (Table 1). These features primarily include the timing of inflection points and peak values, which signify specific phenological phases and growth states. (2) Every year, each sample site's curve should have a consistent form. As an example, if the sample site showed a bimodal signal in 2001 and 2010 but a single-modal signal in 2020, indicating a shift in planting structure, the sample was excluded [5]. Finally, a total of 1548 pixels were selected as the classification samples, including 32 winter wheat–summer maize sample points (Figure 1c) and 48 winter wheat–rice sample points (Figure 1d), which were added based on the Landsat method.

### 2.4.3. Scheme Design

There are only two main crop rotation patterns in the NCP: winter wheat–summer maize and winter wheat–rice. However, land fragmentation and farmers’ autonomous selection of crop types—such as cotton, peanut, soybean, etc.—combined with winter wheat–summer maize MODIS grid units can also result in NDVI curves with bimodal signals. In order to distinguish them from these two pure double-cropping systems, “other double-cropping systems” were developed. Given that spring maize and cotton are representative examples of single-cropping systems, their NDVI curves exhibit distinct variations compared to double-cropping systems. Consequently, we classified them as two distinct categories. Since fruit tree systems such as pear and peach represent typical patterns in the NCP [55] and exhibit a similar NDVI curve, they are considered a single category. Therefore, the classified samples were categorized into six distinct groups: winter wheat–summer maize, winter wheat–rice, spring maize, cotton, other double-cropping systems, and fruit trees. Within each category, we randomly chose 70% of the samples for training the classifier, while the remaining samples were adopted to assess the findings [56]. The information is shown in Table 4.

**Table 4.** The number of training samples and validation samples.

Category	Training Samples (70%)	Validation Samples (30%)	Sum
Winter wheat–summer maize	400	172	572
Winter wheat–rice	251	107	358
Spring maize	116	49	165
Cotton	111	48	159
Other double-cropping systems	104	44	148
Fruit trees	102	44	146

Three different categorization methods were devised in accordance with the categories of the samples (Table 5). In Scheme 1, all six classified samples were comprehensively taken into account. In contrast, Scheme 2 omitted the consideration of the mixed cropping system, a factor typically overlooked in previous studies [31,38]. Similarly, Scheme 3 excluded the winter wheat–rice planting system, which has not been addressed in previous research. Consequently, the winter wheat–rice and mixed cropping systems shown in Scheme 2 and Scheme 3 may be erroneously categorized [57].

**Table 5.** The categorization systems used in the study.

Scheme	Sample Categories
Scheme 1 (S1)	winter wheat–summer maize; winter wheat–rice; spring maize; cotton; other double-cropping systems; fruit trees
Scheme 2 (S2)	5 categories (without the “Other double-cropping systems”)
Scheme 3 (S3)	5 categories (without the “Winter wheat–rice”)

### 2.4.4. Landsat Planting Area Extraction

The spatial resolution of Landsat is 30 m × 30 m, which is much smaller than the area of the study plot. Thus, the distribution of winter wheat–summer maize and winter wheat–rice can be accurately depicted within each image range. The actual area was calculated and summarized using the area statistics tool of ArcMap 10.2, and the basic principle is the number of pixels multiplied by the area of a single pixel. In April, on the collection date of each image, the NDVI value of winter wheat was higher than that of other crops due to the vigorous growth of winter wheat, while other one-season crops, like spring maize, cotton, and fruit trees, had not yet been sown or had not sprouted [16]. The growing period of rice is longer than that of summer maize, and the NDVI value of rice is significantly higher than that of summer maize around September, making the threshold method a simple and

effective method for the small-scale interpretation of winter wheat fields [5]. This can be realized by the decision tree classification tool in ENVI 5.3. The decision tree recognition model is displayed in Figure 2. The main rules of Landsat threshold classification are as follows. (1) Winter wheat is distinguished on the basis that any NDVI value near the first wave peak of winter wheat–summer maize and winter wheat–rice planting systems is significantly larger than that of other planting structures. The criterion is  $\forall \text{NDVI}t_1 \geq 0.6$  ( $\forall$  is a mathematical symbol meaning arbitrary), where  $t_1 \in [2 \text{ April}, 30 \text{ April}]$ . (2) Based on the first criterion, the effective differentiation of the winter wheat–rice and winter wheat–summer maize cropping systems may be determined by assessing if any NDVI value of the former is considerably greater than that of the latter between 7 September and 6 October. The criterion of winter wheat–summer maize is  $\forall \text{NDVI}t_2 \in [0.32, 0.47]$ , and for winter wheat–rice, it is  $\forall \text{NDVI}t_2 \in [0.55, 0.67]$ , where  $t_2 \in [7 \text{ September}, 6 \text{ October}]$ .

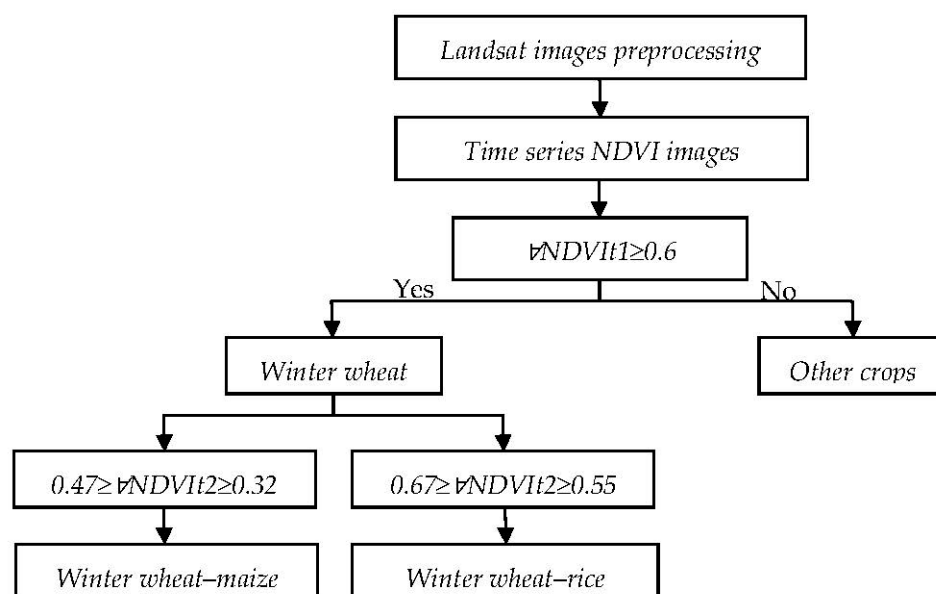


**Figure 2.** The decision tree recognition model for winter wheat–maize and winter wheat–rice.

#### 2.4.5. Accuracy Evaluation

The evaluation of the spatial distribution of winter wheat and summer maize between 2001 and 2020 was conducted at multiple scales, including pixel, county, and regional levels. The confusion matrix approach was employed to illustrate the correlation between the classification outcomes and sampling points [58,59]. Among these, the concept of “overall accuracy” is determined by the division of the aggregate count of pixels correctly categorized by the entire number of pixels included in the matrix [60]. On the other hand, “user’s accuracy” denotes the likelihood that pixels identified on the map accurately reflect the corresponding category on the actual ground. The “producer’s accuracy” shows the chance that a reference pixel is accurately classified [61]. The kappa coefficient is a commonly used metric for assessing accuracy, since it quantifies the degree of consistency remaining after removing unintentional consistency [60,61]. A kappa value over 0.8 signifies a substantial degree of concordance or accuracy between the classification map and the reference data. A coefficient ranging from 0.4 to 0.8 shows a moderate level of agreement, while a coefficient below 0.4 suggests a low level of agreement [54]. At the county scale, a direct comparison was made between the extracted data and the statistical data. At the regional level, Landsat-extracted areas in Julu County and Huaiyin District were validated against statistical areas and employed as a reference to compare with MODIS-extracted areas. The evaluation was performed using R squared ( $R^2$ , the linear regression model’s determination coefficient) and  $p$ -values (to evaluate the significance of the regression

model), and root mean square error (RMSE) was adopted for the evaluation. RMSE was computed using the following formula [5,57]:

$$\text{RMSE} = \sqrt{\frac{1}{n} \sum_{i=1}^n (S_i - O_i)^2} \quad (3)$$

where  $S_i$  represents the  $i$ th extracted area of the planting system,  $O_i$  represents the  $i$ th statistical area of the planting system, and  $n$  indicates the total number of matched statistical and extracted data points.

### 3. Results

#### 3.1. NDVI Curve Characteristics of Typical Crops

Although the MODIS NDVI product MOD3Q1 is composited through the maximum synthesis method, there are still residual errors. The S-G filtering method has been proven effective in improving data quality [46,50]. The pre-processed 12 Landsat images could meet the research requirements. The NDVI time series associated with the field survey points in 2020 were extracted, and the average NDVI values of the training sample points in each category were utilized as their typical NDVI. Taking winter wheat–summer maize and spring maize as representative single- and double-cropping systems, Figure 3 shows the NDVI curves before and after filtering, illustrating the effective fitting of the original NDVI curves at their inflection points. The curves exhibit a generally smooth pattern, aligning with the typical growth pattern of vegetation.

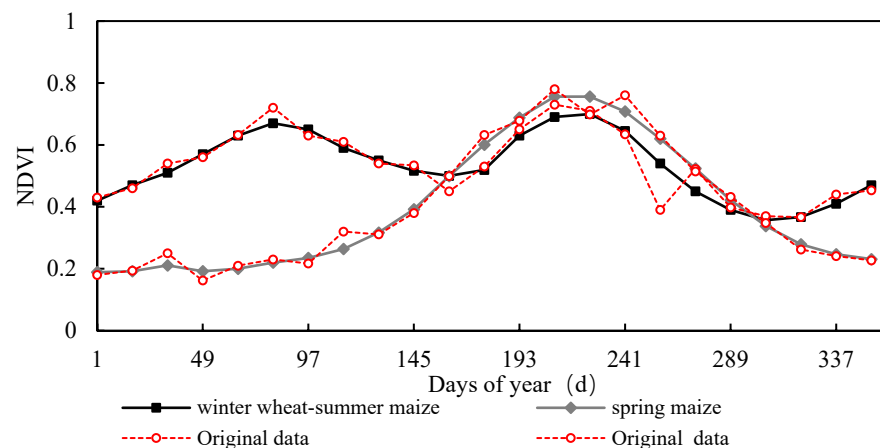


**Figure 3.** NDVI curves of winter wheat–summer maize and spring maize before and after filtering.

The NDVI timing curves of the main planting systems after S-G filtering were presented in Figure 4, which showed that different cropping systems exhibited distinctive curve characteristics. The critical growth phases listed in Table 1 align with the inflection points seen on the NDVI curves of different crops. Winter wheat–summer maize, winter wheat–rice, and “other double cropping systems” exhibit two apparent NDVI peaks. Notably, winter wheat–summer maize and winter wheat–rice share a similar timing for these two NDVI peaks, occurring in late April and early August, respectively. Regarding the senescence date of winter wheat–rice, this occurs in early November, roughly thirty days later than that of winter wheat–summer maize. While the NDVI curve of the “other double-cropping” system exhibits two peaks, the initial peak is notably lower in amplitude compared to that of winter wheat–summer maize and winter wheat–rice distribution, aligning with the findings of Li and Lei [5]. This is due to the bimodal structure of the “other double-cropping systems”, which is caused by the averaging of multiple mixed pixels. The specific reasons for this can be found in the results of Li and Lei [5]. For one cropping system, the initiation period for spring maize spans from 23 April to 8 May, while its senescence phase occurs between 30 September and 16 October. In comparison, cotton

exhibits an earlier planting schedule by approximately one week and a delayed harvesting period by roughly three weeks when compared to spring maize. Fruit trees commence bud bursts in mid-to-late March, with leaf fall occurring in November. Their growth period is notably longer than that of spring maize and cotton.

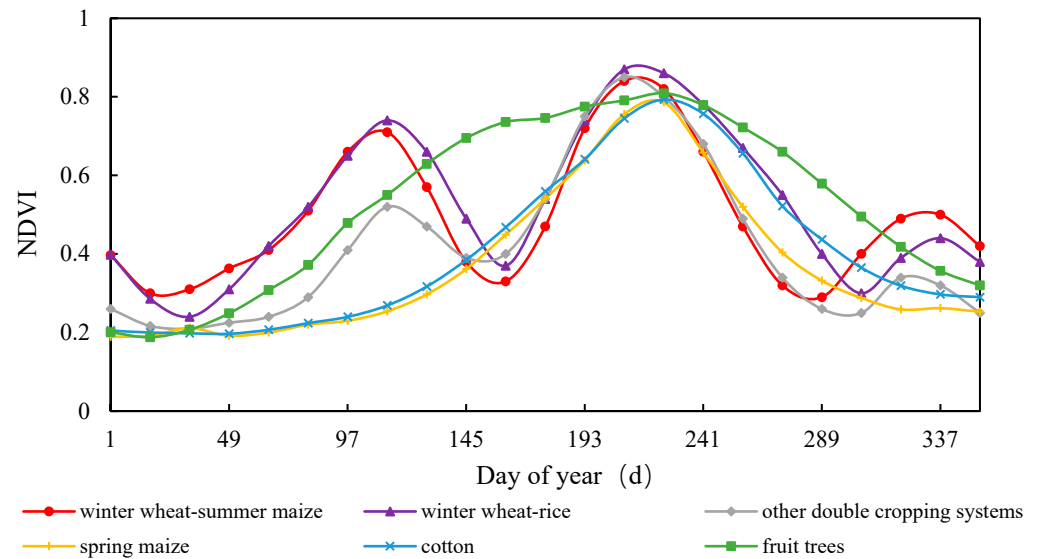


**Figure 4.** NDVI time series curves of the major crops.

3.2. Accuracy Evaluation of Classification Results

At the pixel scale, the confusion matrix for winter wheat–summer maize between 2001 and 2020 was constructed by comparing the extracted results with validation samples (Table 6). Generally speaking, these four classification accuracy evaluation indicators for 2020 were better than those of 2001 and 2010. Although Scheme 3 had marginally greater overall accuracy and kappa coefficient compared to Scheme 2 and Scheme 2 showed a modest superiority over Scheme 1, all three schemes produced average overall accuracy values and kappa coefficients exceeding 87% and 0.85, respectively, for the years 2001, 2010, and 2020. The producer’s accuracy of winter wheat–summer maize in all schemes was above 94%, and the user’s accuracy was above 87% in all schemes. The findings of the confusion matrix indicate that all three schemes exhibited satisfactory accuracy in their classification results.

**Table 6.** The confusion matrix of winter wheat–summer maize.

Year	Scheme	Overall Accuracy (%)	Kappa Coefficient	Producer’s Accuracy (%)	User’s Accuracy (%)
2001	S1	87.43	83.50	98.03	86.19
	S2	88.89	84.76	94.12	89.14
	S3	89.75	87.89	96.92	87.27
2010	S1	93.22	83.34	93.17	94.08
	S2	93.80	85.11	95.87	93.05
	S3	94.35	86.38	95.12	92.17
2020	S1	95.93	93.24	95.26	93.32
	S2	96.48	93.93	97.17	92.18
	S3	97.32	94.67	94.32	94.39

At the county level,  $R^2$  values for the three schemes from 2001 to 2020 exceeded 0.7 (Figures 5–7). While the  $R^2$  values for Scheme 2 (Figures 5b, 6b and 7b) were marginally higher than those of Schemes 3 (Figures 5c, 6c and 7c) and 1 (Figures 5a, 6a and 7a), this resulted in a significantly greater RMSE, indicating a noticeable overestimation of the

winter wheat–summer maize cultivation area in Scheme 2. The MODIS-extracted data from Scheme 1 of the six sample categories yielded the best results when compared to the statistical data, with an RMSE of 179.05 to 215.72 km<sup>2</sup>. In all years of the three schemes, the cultivation areas extracted from MODIS datasets were greater than the statistical data, as confirmed by previous studies [5,21,62], mainly due to various political and policy factors. Official statistics related to cultivated land taxes and grain production quotas underestimate the planted areas of winter wheat–summer maize [21,63,64].

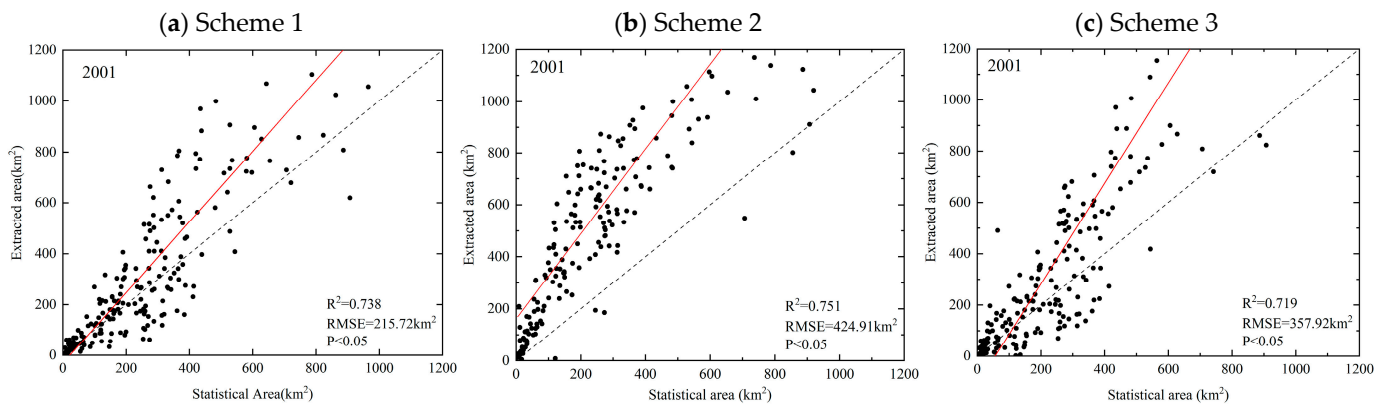


Figure 5. Accuracy evaluation of county classification results from 2001.

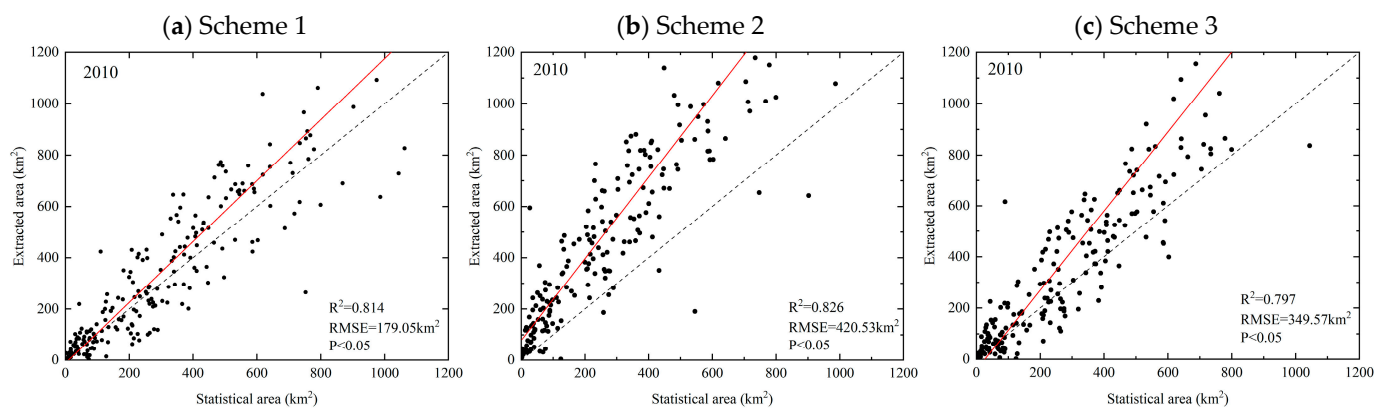


Figure 6. Accuracy evaluation of county classification results from 2010.

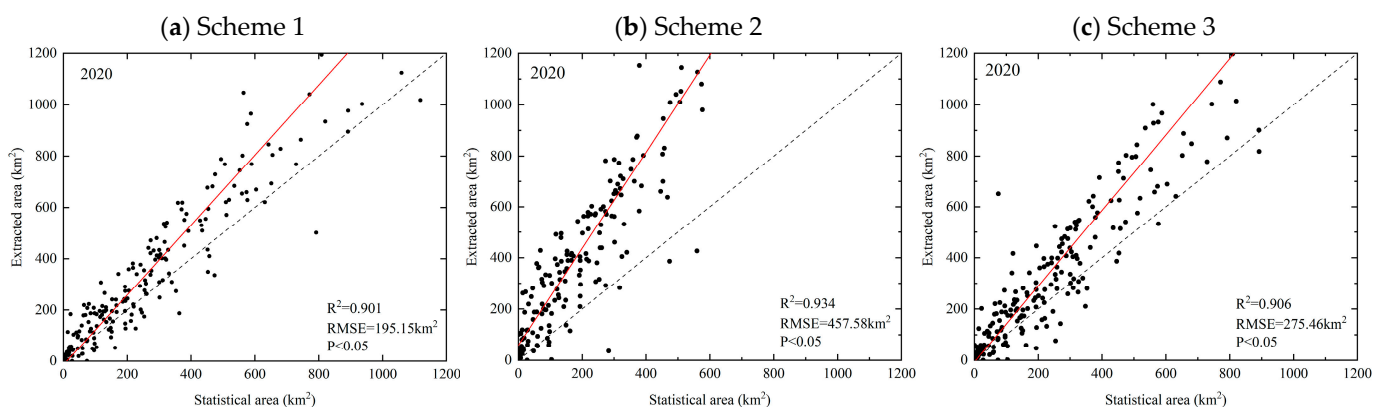


Figure 7. Accuracy evaluation of county classification results from 2020.

At a regional scale, the total areas extracted from Landsat images for winter wheat–summer maize and winter wheat–rice in Julu County and Huaiyin District between 2001

and 2020 are shown in Table 7. Except for an 89% extraction accuracy in Julu County in 2001, all accuracy values reached more than 90%, which was generally in good agreement with the statistical results. This accurately reflects the regional planting patterns of winter wheat–summer maize and winter wheat–rice.

**Table 7.** Comparison of Landsat extraction areas and statistical areas.

Region	Year	Statistical Area (km <sup>2</sup> )	Extracted Area (km <sup>2</sup> )	Accuracy (%)
Julu County	2001	154.00	172.66	89.19
	2010	158.85	153.57	96.68
	2020	187.36	203.36	92.13
Huaiyin District	2001	252.13	233.65	92.67
	2010	447.75	455.4	98.32
	2020	503.85	537.27	93.78

A fitting analysis was performed between the Landsat extraction areas and MODIS results at the township level to assess MODIS extraction accuracy on a regional scale, as depicted in Figure 8. In general, the fitting accuracy in Huaiyin District surpassed that in Julu County. The  $R^2$  values for both of these regions exceeded 0.8, with RMSE values ranging between 4.21 km<sup>2</sup> and 7.05 km<sup>2</sup>, signifying a solid overall correlation between the Landsat and MODIS extraction results. Nevertheless, the MODIS results significantly overestimate the planting areas for winter wheat–summer maize and winter wheat–rice. This trend aligns with the findings from the county-level assessment.

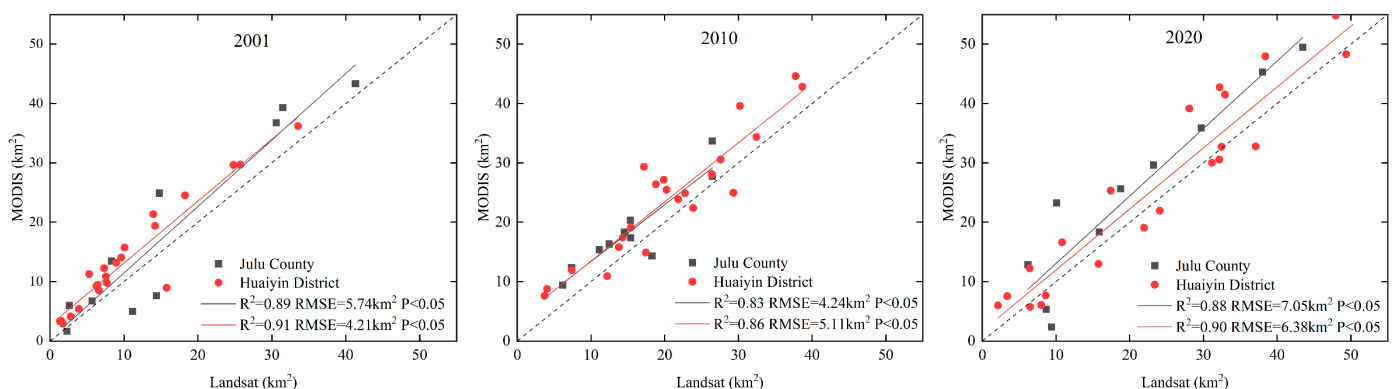


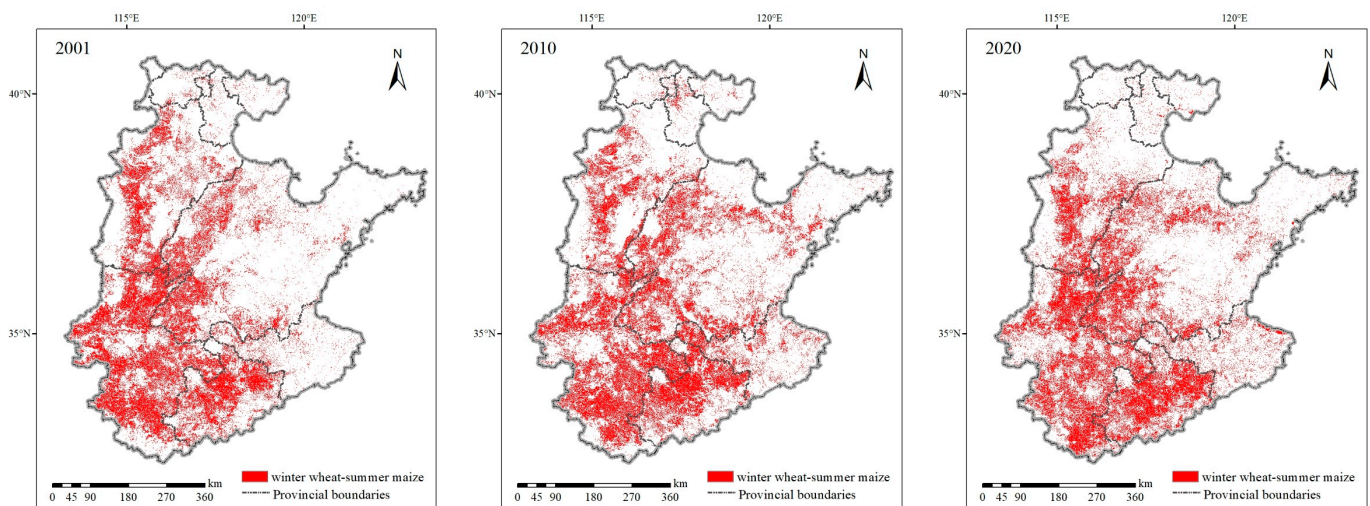
**Figure 8.** Comparison of winter wheat–summer maize and wheat wheat–rice planting area extracted from MODIS data and Landsat images from 2001, 2010, and 2020.

### 3.3. Temporal and Spatial Changes in Winter Wheat–Summer Maize Distribution

Regarding the overall NCP, the planting area of winter wheat–summer maize between 2001 and 2020 demonstrated a significant inter-annual fluctuation (Table 8). The comparative analysis shown in Figure 9 reveals that the cultivation of winter wheat–summer maize was predominantly concentrated in the middle of the Hebei Plain, along the Yellow River irrigation areas and humid zones of the southwest NCP, accounting for 75–85% of the total NCP planting area. The sown area of winter wheat–summer maize exhibited a consistent rising trend, increasing from  $14.17 \times 10^4$  km<sup>2</sup> in 2001 to  $17.49 \times 10^4$  km<sup>2</sup> in 2020 (Table 8), representing a growth of  $3.32 \times 10^4$  km<sup>2</sup> (23.43%). From 2001 to 2010, this area increased by  $1.75 \times 10^4$  km<sup>2</sup> (12.35%), equating to an average annual increase of 1800 km<sup>2</sup>. The cultivated area of winter wheat–summer maize expanded by  $1.57 \times 10^4$  km<sup>2</sup> (9.86%) between 2011 and 2020, demonstrating an average annual increase of 1700 km<sup>2</sup>, a rate lower than that observed from 2001 to 2010.

**Table 8.** Changes in winter wheat–summer maize sowing area at the provincial level in the NCP.

Region	Area and Percentage of Winter Wheat–Summer Maize					
	Year of 2001		Year of 2010		Year of 2020	
	Area/km <sup>2</sup>	Percentage/%	Area/km <sup>2</sup>	Percentage/%	Area/km <sup>2</sup>	Percentage/%
Beijing	939.31	0.66	595.20	0.37	541.15	0.31
Tianjin	1258.06	0.89	1160.43	0.73	673.58	0.39
Hebei	27,458.82	19.38	23,347.25	14.68	25,459.33	14.56
Henan	49,717.73	35.09	52,918.62	33.27	56,689.48	32.41
Shandong	35,873.6	25.32	46,152.24	29.01	54,623.88	31.23
Jiangsu	4787.73	3.38	10,972.28	6.90	9165.81	5.24
Anhui	21,663.91	15.29	23,932.40	15.04	27,753.77	15.87
North China Plain	141,699.16	100	159,078.42	100	174,907.00	100

**Figure 9.** Spatio-temporal changes in the winter wheat–summer maize sowing area in the NCP in 2001, 2010, and 2020.

From the perspective of county-level administrative units (Figure 10), major counties with winter wheat–summer maize cultivation areas exceeding 300 km<sup>2</sup> in the NCP are primarily situated in the central part of Hebei province (Shijiazhuang, Hengshui, and Xingtai cities); the northwestern part of Shandong province (Dezhou and Liaocheng cities); Heze in the southwestern region; the Jiaolai Plain; areas in the eastern and southern parts of Henan; and the northern part of Anhui. Remarkably, in the southern part of Henan and the northern part of Anhui, more than 70% of counties had planting areas exceeding  $6 \times 10^4$  km<sup>2</sup> between 2001 and 2020, forming the most significant spatial clustering of winter wheat–summer maize in the NCP.

From 2001 to 2020, there was a fluctuating upward trend in the size of winter wheat–summer maize planting areas in Henan’s eastern and southern regions, Shandong’s northern regions, the Jiaolai Plain, the northern plain of Anhui, and the northern plain of Jiangsu (Figure 11). In contrast, the counties within the Beijing–Tianjin–Hebei region experienced reduced fluctuations in planting areas of winter wheat–summer maize. Specifically, a notable decline was seen between 2001 and 2010, followed by a minor resurgence in the cultivation of winter wheat–summer maize from 2010 to 2020. This pattern aligns with the findings reported by Wang et al. [6].

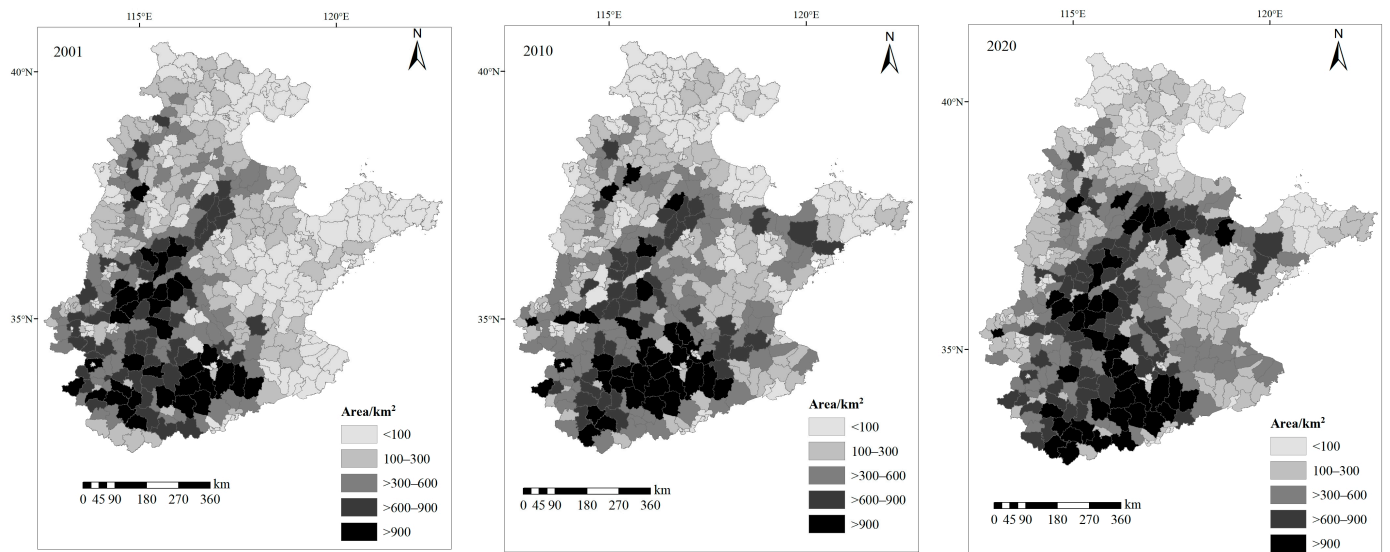


**Figure 10.** Planting areas of winter wheat–summer maize at the county level in the NCP in 2001, 2010, and 2020.

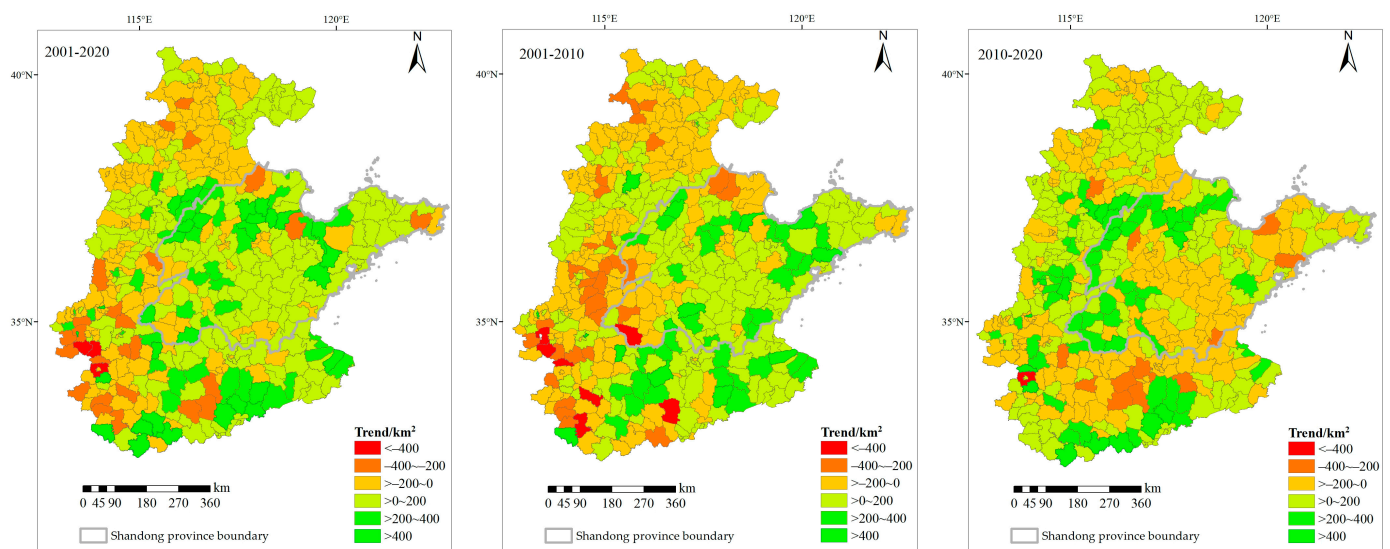


**Figure 11.** Spatial variation trend in winter wheat–summer maize planting area during 2001–2020, 2001–2010, and 2010–2020 at the county level.

#### 4. Discussion

Given the phenological similarities between the winter wheat–summer maize and winter wheat–rice planting systems, we incorporated winter wheat–rice sample points into the classification category to alleviate the potential interference from the winter wheat–rice cropping system. Due to the NCP’s decentralized and autonomous farming practices, mixed cropping patterns involving winter wheat alongside crops such as cotton, peanut, and soybean are prevalent. Therefore, other double-cropping systems were established. When comparing the three schemes, both Scheme 2 and Scheme 3 significantly overestimated the area of winter wheat–summer maize. Notably, the overestimation in Scheme 2 exceeded that in Scheme 3, signifying that the absence of other double-cropping systems introduced a higher degree of uncertainty. Due to the bimodal signals created by mixed crops and the winter wheat–rice grid being misclassified into the winter wheat–summer maize category, the distribution of winter wheat–summer maize was overestimated. The results indicate that the extracted accuracy of winter wheat–summer maize distributions

could be significantly improved by considering the mixed-pixel “other double-cropping systems” and “double-cropping model” of winter wheat–rice.

The extracted winter wheat–summer maize areas were compared with those of previous studies. Li and Lei [5] estimated the sown area of winter wheat–summer maize in the NCP between 2001 and 2018, and the extracted results in 2001 and 2010 were 9.39% and 11.82% higher than those in our study, respectively. This may be due to these two studies using the Savitzky–Golay filtering and harmonic analysis methods to smooth and rebuild the NDVI time series, respectively. In addition, our study enriched pure winter wheat–rice sample points based on Landsat images from major rice-producing areas, which could better distinguish the NDVI time series characteristics of winter wheat–summer maize and reduce the probability of winter wheat–rice being misclassified as winter wheat–summer maize to a certain extent. Wang et al. [6] estimated the winter wheat planting areas of the NCP in 2001, 2006, and 2011, and the results for 2001 and 2011 were 26.39% and 24.69% lower than those from our study for 2001 and 2010, respectively. In their research, the second-order difference approach was used to isolate the peaks and valleys of EVI curves, and the identification rules were formulated based on the key phases by combining two Landsat regions. However, there were still abnormal fluctuations in the EVI curve after smoothing, which may lead to the extraction of pseudo-peaks or pseudo-valleys [21], resulting in the excessive removal of winter wheat. Guo [65] extracted winter wheat distribution data in the Huang-Huai-hai region based on the global optimization threshold algorithm of total quantity control. At the provincial level, the extraction results for Shandong, Henan, and Hebei for 2001 were 7.14%, 25.38%, and 10.35% lower than those in our study, and the extraction results for 2010 were 11.39%, 25.43%, and 0.45% lower than those in our study, respectively. This may be because the uncertainty of threshold values causes the uncertainty of the winter wheat–summer maize cultivation area [66], and the mixed-pixel problem of MODIS images was not considered.

The sown area of winter wheat–summer maize in the NCP from 2001 to 2020 demonstrated an overall trend of increasing by 12.35% from 2001 to 2010 and 9.86% from 2011 to 2020. From 2001 to 2010, there was a significant inter-annual fluctuation at the province level, with planting areas decreasing in Beijing, Tianjin, and Hebei. Meanwhile, the opposite trend was observed for Shandong, Jiangsu, Anhui, and Henan, which was essentially consistent with previous studies [5,6,33,65]. The increase in irrigation costs caused by the decrease in groundwater levels in the Beijing–Tianjin–Hebei region and the increase in labor cost associated with the transfer of labor from agriculture may be the leading causes [6,67]. Between 2011 and 2020, the planting area of winter wheat–summer maize increased in Hebei, Henan, Anhui, and Shandong, while it decreased in Beijing and Tianjin and slightly reduced in Jiangsu. With the introduction of policies such as the exemption of agricultural tax, issuance of agricultural subsidies, and the minimum purchase price of agricultural products [68], the planting of winter wheat–summer maize in the southern part of the Hebei Plain resumed. On the other hand, there was an expansion of winter wheat–summer maize cultivation in irrigated regions along the Yellow River and the Jiaolai Plain within Shandong province, which were recognized as significant cotton-producing areas, characterized by labor-intensive cotton cultivation and management practices in comparison to winter wheat–summer maize [69]. With rising labor costs and persistently low cotton prices, some farmers abandoned cotton planting and switched to winter wheat–summer maize [21]. In the southern sector of the NCP, the overall planting area of winter wheat–summer maize significantly expanded. This expansion could be attributed to several factors, including higher precipitation levels in the region, resulting in lower irrigation costs than those for the Beijing–Tianjin–Hebei region. Additionally, the advanced state of agricultural mechanization in winter wheat–summer maize planting has modernized agricultural labor and thus contributed to lower costs [70].

## 5. Conclusions

This study revealed the spatial-temporal variation in the NCP's winter wheat–summer maize planting structure between 2001 and 2020. The MOD13Q1 product, with a temporal resolution of 16 days and a spatial resolution of 0.0025°, is capable of producing accurate identification results in this region. In terms of establishing sample categories, six sample categories—winter wheat–summer maize, winter wheat–rice, other double-cropping systems, spring maize, cotton, and fruit trees—could significantly improve the recognition accuracy of winter wheat–summer maize distribution, with  $R^2$  and RMSE values ranging from 0.738 to 0.901 and from 179.05 to 215.72 km<sup>2</sup>, respectively. The absence of mixed systems or winter wheat–rice distribution diminished the effectiveness of identifying winter wheat–summer maize, among which the former had a more significant effect on the classification results.

From 2001 to 2020, the planting area declined by 2982.13 km<sup>2</sup> (10.06%) in the northern part of the NCP, including the Beijing–Tianjin–Hebei region, while it increased by  $3.62 \times 10^4$  km<sup>2</sup> (32.30%) in the middle and southern part, encompassing Shandong, Henan, Anhui, and Jiangsu provinces. The winter wheat–summer maize growing region was concentrated mostly in the middle of the Hebei Plain, along the Yellow River irrigation areas, and in humid zones of the southwest NCP. This region accounted for 75–85% of the total NCP planting area. These results are significant for crop production, groundwater protection, and the management of agricultural water resources in this region. Optimization of planting structures based on agricultural water resources will be the focus of our subsequent research.

**Author Contributions:** Conceptualization, B.Y., X.H. and J.W.; methodology, S.L. and B.Y.; validation, S.L.; investigation, B.Y. and S.L.; writing—original draft preparation, B.Y.; writing—review and editing, S.L., B.Y., X.H. and J.W. All authors have read and agreed to the published version of the manuscript.

**Funding:** This research was funded by the Central Public-interest Scientific Institution Basal Research Fund (Grant No. IFI2023-30).

**Data Availability Statement:** The links to the foundational data required for this study can be found within the article. In addition, the data presented in this study are available on request from the corresponding author.

**Acknowledgments:** The authors would like to thank the anonymous reviewers for their helpful comments that improved the manuscript.

**Conflicts of Interest:** The authors declare no conflict of interest.

## References

1. Xu, Z.; Chen, X.; Liu, J.; Zhang, Y.; Chau, S.; Bhattarai, N.; Wang, Y.; Li, Y.; Connor, T.; Li, Y. Impacts of irrigated agriculture on food–energy–water–CO<sub>2</sub> nexus across metacoupled systems. *Nat. Commun.* **2020**, *11*, 5837. [[CrossRef](#)] [[PubMed](#)]
2. Li, Z.; Yang, P.; Zhou, Q.; Wang, Y.; Wu, W.; Zhang, L.; Zhang, X. Research on spatiotemporal pattern of crop phenological characteristics and cropping system in North China based on NDVI time series data. *Acta Ecol. Sin.* **2009**, *29*, 6216–6226.
3. Tao, F.; Xiao, D.; Zhang, S.; Zhang, Z.; Rötter, R.P. Wheat yield benefited from increases in minimum temperature in the Huang-Huai-Hai Plain of China in the past three decades. *Agric. For. Meteorol.* **2017**, *239*, 1–14. [[CrossRef](#)]
4. Wang, S.; Hu, Y.; Yuan, R.; Feng, W.; Pan, Y.; Yang, Y. Ensuring water security, food security, and clean water in the North China Plain—conflicting strategies. *Curr. Opin. Environ. Sustain.* **2019**, *40*, 63–71. [[CrossRef](#)]
5. Li, J.; Lei, H. Tracking the spatio-temporal change of planting area of winter wheat–summer maize cropping system in the North China Plain during 2001–2018. *Comput. Electron. Agric.* **2021**, *187*, 106222. [[CrossRef](#)]
6. Wang, X.; Li, X.; Tan, M.; Xin, L. Remote sensing monitoring of changes in winter wheat area in North China Plain from 2001 to 2011. *Trans. Chin. Soc. Agric. Eng.* **2015**, *31*, 190–199.
7. Mo, X.-G.; Hu, S.; Lin, Z.-H.; Liu, S.-X.; Xia, J. Impacts of climate change on agricultural water resources and adaptation on the North China Plain. *Adv. Clim. Chang. Res.* **2017**, *8*, 93–98. [[CrossRef](#)]
8. Wu, D.; Fang, S.; Li, X.; He, D.; Zhu, Y.; Yang, Z.; Xu, J.; Wu, Y. Spatial-temporal variation in irrigation water requirement for the winter wheat–summer maize rotation system since the 1980s on the North China Plain. *Agric. Water Manag.* **2019**, *214*, 78–86. [[CrossRef](#)]

9. Yang, X.; Wang, G.; Chen, Y.; Sui, P.; Pacenka, S.; Steenhuis, T.S.; Siddique, K.H.M. Reduced groundwater use and increased grain production by optimized irrigation scheduling in winter wheat–summer maize double cropping system—A 16-year field study in North China Plain. *Field Crops Res.* **2022**, *275*, 108364. [[CrossRef](#)]
10. Jin, M.G.; Zhang, R.Q.; Sun, L.F.; Gao, U.F. Temporal and spatial soil water management: A case study in the Heilonggang region, PR China. *Agric. Water Manag.* **1999**, *42*, 173–187. [[CrossRef](#)]
11. Wu, X.; Yang, W.; Wang, C.; Shen, Y.; Kondoh, A. Interactions among the Phenological Events of Winter Wheat in the North China Plain—Based on Field Data and Improved MODIS Estimation. *Remote Sens.* **2019**, *11*, 2976. [[CrossRef](#)]
12. Liu, J.; Si, Z.; Wu, L.; Shen, X.; Gao, Y.; Duan, A. High-low seedbed cultivation drives the efficient utilization of key production resources and the improvement of wheat productivity in the North China Plain. *Agric. Water Manag.* **2023**, *285*, 108357. [[CrossRef](#)]
13. Yang, X.; Chen, Y.; Pacenka, S.; Gao, W.; Ma, L.; Wang, G.; Yan, P.; Sui, P.; Steenhuis, T.S. Effect of diversified crop rotations on groundwater levels and crop water productivity in the North China Plain. *J. Hydrol.* **2015**, *522*, 428–438. [[CrossRef](#)]
14. Sun, H.; Shen, Y.; Yu, Q.; Flerchinger, G.N.; Zhang, Y.; Liu, C.; Zhang, X. Effect of precipitation change on water balance and WUE of the winter wheat–summer maize rotation in the North China Plain. *Agric. Water Manag.* **2010**, *97*, 1139–1145. [[CrossRef](#)]
15. Franch, B.; Vermote, E.F.; Becker-Reshef, I.; Claverie, M.; Huang, J.; Zhang, J.; Justice, C.; Sobrino, J.A. Improving the timeliness of winter wheat production forecast in the United States of America, Ukraine and China using MODIS data and NCAR Growing Degree Day information. *Remote Sens. Environ.* **2015**, *161*, 131–148. [[CrossRef](#)]
16. Skakun, S.; Vermote, E.; Roger, J.-C.; Franch, B. Combined Use of Landsat-8 and Sentinel-2A Images for Winter Crop Mapping and Winter Wheat Yield Assessment at Regional Scale. *AIMS Geosci.* **2017**, *3*, 163–186. [[CrossRef](#)]
17. Zhang, J.; Cheng, Y.; Zhang, F. Crops planting information extraction based on multi-temporal remote sensing images. *Trans. CSAE* **2012**, *28*, 134–141.
18. Atzberger, C. Advances in Remote Sensing of Agriculture: Context Description, Existing Operational Monitoring Systems and Major Information Needs. *Remote Sens.* **2013**, *5*, 949–981. [[CrossRef](#)]
19. Tang, K.Y.; Wang, X.; Wan, Q.H.; Fang, S.G. A crucial role of paralogous beta-defensin genes in the Chinese alligator innate immune system revealed by the first determination of a Crocodilia defensin cluster. *Dev. Comp. Immunol.* **2018**, *81*, 193–203. [[CrossRef](#)]
20. Tian, F.; Wu, B.; Zeng, H.; Zhang, X.; Xu, J. Efficient Identification of Corn Cultivation Area with Multitemporal Synthetic Aperture Radar and Optical Images in the Google Earth Engine Cloud Platform. *Remote Sens.* **2019**, *11*, 629. [[CrossRef](#)]
21. Yan, H.; Liu, F.; Qin, Y.; Niu, Z.E.; Doughty, R.; Xiao, X. Tracking the spatio-temporal change of cropping intensity in China during 2000–2015. *Environ. Res. Lett.* **2019**, *14*, 035008. [[CrossRef](#)]
22. Becker-Reshef, I.; Vermote, E.; Lindeman, M.; Justice, C. A generalized regression-based model for forecasting winter wheat yields in Kansas and Ukraine using MODIS data. *Remote Sens. Environ.* **2010**, *114*, 1312–1323. [[CrossRef](#)]
23. Yang, Y.; Tao, B.; Ren, W.; Zourarakis, D.P.; Masri, B.E.; Sun, Z.; Tian, Q. An Improved Approach Considering Intra-class Variability for Mapping Winter Wheat Using Multitemporal MODIS EVI Images. *Remote Sens.* **2019**, *11*, 1191. [[CrossRef](#)]
24. Jiang, L.; Wang, P.; Jiang, L.; Gong, L.; Yu, C.; Li, X. Estimation of Crop Planting Area and Spatial Distribution Based on MODIS NDVI Time-series Data of Rice and Dry Farmland Crops. *Chin. Agric. Sci. Bull.* **2021**, *37*, 108–118.
25. Dong, J.; Xiao, X. Evolution of regional to global paddy rice mapping methods: A review. *ISPRS J. Photogramm. Remote Sens.* **2016**, *119*, 214–227. [[CrossRef](#)]
26. Zhang, G.; Xiao, X.; Biradar, C.M.; Dong, J.; Qin, Y.; Menarguez, M.A.; Zhou, Y.; Zhang, Y.; Jin, C.; Wang, J.; et al. Spatiotemporal patterns of paddy rice croplands in China and India from 2000 to 2015. *Sci. Total Environ.* **2017**, *579*, 82–92. [[CrossRef](#)]
27. Hao, W.; Mei, X.; Cai, X.; Du, J.; Liu, Q. Crop planting extraction based on multi-temporal remote sensing data in Northeast China. *Trans. CSAE* **2011**, *27*, 201–207.
28. Chen, Y.; Lu, D.; Moran, E.; Batistella, M.; Dutra, L.V.; Sanches, I.D.A.; da Silva, R.F.B.; Huang, J.; Luiz, A.J.B.; de Oliveira, M.A.F. Mapping croplands, cropping patterns, and crop types using MODIS time-series data. *Int. J. Appl. Earth Obs. Geoinf.* **2018**, *69*, 133–147. [[CrossRef](#)]
29. García-Mora, T.J.; Mas, J.-F.; Hinkley, E.A. Land cover mapping applications with MODIS: A literature review. *Int. J. Digit. Earth* **2012**, *5*, 63–87. [[CrossRef](#)]
30. Yu, B.; Shang, S. Multi-Year Mapping of Maize and Sunflower in Hetao Irrigation District of China with High Spatial and Temporal Resolution Vegetation Index Series. *Remote Sens.* **2017**, *9*, 855. [[CrossRef](#)]
31. Zhang, M.; Zhou, Q.; Chen, Z.; Liu, J.; Zhou, Y.; Cai, C. Crop discrimination in Northern China with double cropping systems using Fourier analysis of time-series MODIS data. *Int. J. Appl. Earth Obs. Geoinf.* **2008**, *10*, 476–485.
32. Zhang, Y.; Guo, Y.; Shen, Y.; Qi, Y.; Luo, J. Impact of planting structure changes on agricultural water requirement in North China Plain. *Chin. J. Eco-Agric.* **2020**, *28*, 8–16.
33. Pan, X.; Li, G.; Liu, F.; Wu, X.; Kondoh, A.; Shen, Y. Using remote sensing to determine spatio-temporal variations in winter wheat growing area in the North China Plain. *Chin. J. Eco-Agric.* **2015**, *23*, 497–505.
34. Zhang, W.; Brandt, M.; Prishchepov, A.V.; Li, Z.; Lyu, C.; Fensholt, R. Mapping the Dynamics of Winter Wheat in the North China Plain from Dense Landsat Time Series (1999 to 2019). *Remote Sens.* **2021**, *13*, 1170. [[CrossRef](#)]
35. Zhang, Y.; Qi, Y.; Shen, Y.; Wang, H.; Pan, X. Mapping the agricultural land use of the North China Plain in 2002 and 2012. *J. Geogr. Sci.* **2019**, *29*, 909–921. [[CrossRef](#)]

36. Zhang, X.; Shuai, T.; Yang, H.; Huang, C. Winter wheat planting area extraction based on MODIS EVI image time series. *Trans. CSAE* **2010**, *26*, 220–224.
37. Zhang, J.; Feng, L.; Yao, F. Improved maize cultivated area estimation over a large scale combining MODIS–EVI time series data and crop phenological information. *ISPRS J. Photogramm. Remote Sens.* **2014**, *94*, 102–113. [[CrossRef](#)]
38. Wang, P.; Xun, L.; Li, L.; Xie, Y.; Wang, L. Extraction of planting areas of main crops based on Fourier transformed characteristics of time series leaf area index products. *Trans. CSAE* **2017**, *33*, 207–215.
39. Wu, J.; Cheng, G.; Wang, N.; Shen, H.; Ma, X. Spatiotemporal Patterns of Multiscale Drought and Its Impact on Winter Wheat Yield over North China Plain. *Agronomy* **2022**, *12*, 1209. [[CrossRef](#)]
40. Mo, X.; Liu, S.; Lin, Z.; Guo, R. Regional crop yield, water consumption and water use efficiency and their responses to climate change in the North China Plain. *Agric. Ecosyst. Environ.* **2009**, *134*, 67–78. [[CrossRef](#)]
41. UNEP. *World Atlas of Desertification*, 2nd ed.; UNEP: London, UK, 1997.
42. Clark, M.L.; Aide, T.M.; Grau, H.R.; Riner, G. A scalable approach to mapping annual land cover at 250 m using MODIS time series data: A case study in the Dry Chaco ecoregion of South America. *Remote Sens. Environ.* **2010**, *114*, 2816–2832. [[CrossRef](#)]
43. Huete, A.; Didan, K.; Miura, T.; Rodriguez, E.P.; Gao, X.; Ferreira, L.G. Overview of the radiometric and biophysical performance of the MODIS vegetation indices. *Remote Sens. Environ.* **2002**, *83*, 195–213. [[CrossRef](#)]
44. Chen, J.; Chen, L.; Chen, F.; Ban, Y.; Li, S.; Han, G.; Tong, X.; Liu, C.; Stamenov, V.; Stamenov, S. Collaborative validation of Globeland30: Methodology and practices. *Geo-Spat. Inf. Sci.* **2021**, *24*, 134–144. [[CrossRef](#)]
45. Chen, J.; Zhu, X.; Vogelmann, J.E.; Gao, F.; Jin, S. A simple and effective method for filling gaps in Landsat ETM+ SLC-off images. *Remote Sens. Environ.* **2011**, *115*, 1053–1064. [[CrossRef](#)]
46. Bian, J.; Li, A.; Song, M.; Ma, L.; Jang, J. Reconstruction of NDVI time-series datasets of MODIS based on Savitzky-Golay filter. *J. Remote Sens.* **2010**, *14*, 725–741.
47. Ma, M.; Veroustraete, F. Reconstructing pathfinder AVHRR land NDVI time-series data for the Northwest of China. *Adv. Space Res.* **2006**, *37*, 835–840. [[CrossRef](#)]
48. Chen, J.; Jönsson, P.; Tamura, M.; Gu, Z.; Matsushita, B.; Eklundh, L. A simple method for reconstructing a high-quality NDVI time-series data set based on the Savitzky–Golay filter. *Remote Sens. Environ.* **2004**, *91*, 332–344. [[CrossRef](#)]
49. Wang, X.; Wang, Y.; Fang, P.; Qin, F.; Zhang, X. Extraction and temporal and spatial Pattern Analysis of Multiple Cropping Indexes in Henan Province Based on time Series MODIS NDVI. *J. Henan Univ. Nat. Sci.* **2020**, *50*, 524–534.
50. Liu, H.; Feng, L.; Zhu, L.; Huang, Y. Performance of Filters for City Region HJ-1A/B NDVI Time-series Analysis. *Remote Sens. Inf.* **2015**, *30*, 69–76.
51. Per, J.; Lars, E. Seasonality Extraction by Function Fitting to Time-Series of Satellite Sensor Data. *IEEE Trans. Geosci. Remote Sens.* **2002**, *40*, 1824–1832.
52. Tang, K.; Zhu, W.; Zhan, P.; Ding, S. An Identification Method for Spring Maize in Northeast China Based on Spectral and Phenological Features. *Remote Sens.* **2018**, *10*, 193. [[CrossRef](#)]
53. Arvor, D.; Jonathan, M.; Meirelles, M.S.P.; Dubreuil, V.; Durieux, L. Classification of MODIS EVI time series for crop mapping in the state of Mato Grosso, Brazil. *Int. J. Remote Sens.* **2011**, *32*, 7847–7871. [[CrossRef](#)]
54. Jensen, J.R.; Lulla, K. Introductory digital image processing: A remote sensing perspective. *Geocarto Int.* **2007**, *2*, 65. [[CrossRef](#)]
55. Yang, T.; Wang, J.; Zhang, H.; Li, R.; Zhang, Y.; Shen, Y. Evapotranspiration of typical agroecosystems in the North China Plain based on single crop coefficient method. *Chin. J. Eco-Agric.* **2022**, *30*, 356–366.
56. Fan, X. *A Research of Extracting Agricultural Growing Areas Informations with FY-3 MERSI Data*; University of Electronic Science and Technology of China: Chengdu, China, 2015.
57. Li, J.; Lei, H. Impacts of climate change on winter wheat and summer maize dual-cropping system in the North China Plain. *Environ. Res. Commun.* **2022**, *4*, 075014. [[CrossRef](#)]
58. Foody, G.M. Status of land cover classification accuracy assessment. *Remote Sens. Environ.* **2002**, *80*, 185–201. [[CrossRef](#)]
59. Olofsson, P.; Foody, G.M.; Herold, M.; Stehman, S.V.; Woodcock, C.E.; Wulder, M.A. Good practices for estimating area and assessing accuracy of land change. *Remote Sens. Environ.* **2014**, *148*, 42–57. [[CrossRef](#)]
60. Congalton, R.G. A review of assessing the accuracy of classifications of remotely sensed data. *Remote Sens. Environ.* **1991**, *37*, 35–46. [[CrossRef](#)]
61. Liu, C.; Frazier, P.; Kumar, L. Comparative assessment of the measures of thematic classification accuracy. *Remote Sens. Environ.* **2007**, *107*, 606–616. [[CrossRef](#)]
62. Luo, Y.; Zhang, Z.; Li, Z.; Chen, Y.; Zhang, L.; Cao, J.; Tao, F. Identifying the spatiotemporal changes of annual harvesting areas for three staple crops in China by integrating multi-data sources. *Environ. Res. Lett.* **2020**, *15*, 074003. [[CrossRef](#)]
63. Xiao, X.M.; Liu, J.Y.; Zhuang, D.F.; Frohling, S.; Boles, S.; Xu, B.; Liu, M.L.; Salas, W.; Moore, B.; Li, C.S. Uncertainties in estimates of cropland area in China: A comparison between an AVHRR-derived dataset and a Landsat TM-derived dataset. *Glob. Planet. Chang.* **2003**, *37*, 297–306. [[CrossRef](#)]
64. Liu, J.; Liu, M.; Tian, H.; Zhuang, D.; Zhang, Z.; Zhang, W.; Tang, X.; Deng, X. Spatial and temporal patterns of China’s cropland during 1990–2000: An analysis based on Landsat TM data. *Remote Sens. Environ.* **2005**, *98*, 442–456. [[CrossRef](#)]
65. Guo, W. *Distribution and Spatial-Temporal Variation of Winter Wheat Based on Integrating of Remote Sensing and Statistical Data*; Chinese Academy of Agricultural Sciences: Beijing, China, 2018.

66. Zhang, S.; Zhang, J.; Bai, Y.; Yao, F. Extracting winter wheat area in Huanghuaihai Plain using MODIS-EVI data and phenology difference avoiding threshold. *Trans. Chin. Soc. Agric. Eng.* **2018**, *34*, 150–158.
67. Xin, L.; Li, X.; Tan, M.; Hao, H. The rise of ordinary labor wage and its effect of agricultural land use in present China. *Geogr. Res.* **2011**, *30*, 1391–1400.
68. Long, H. Land use policy in China: Introduction. *Land Use Policy* **2014**, *40*, 1–5. [[CrossRef](#)]
69. Wu, X.; Qi, Y.; Shen, Y.; Yang, W.; Zhang, Y.; Kondoh, A. Change of winter wheat planting area and its impacts on groundwater depletion in the North China Plain. *J. Geogr. Sci.* **2019**, *29*, 891–908. [[CrossRef](#)]
70. Cai, J.; Tang, Z. The Development of Agricultural Mechanization in North China Plain and the Formation of Agricultural Mechanization Service Market. *Reform* **2016**, *10*, 65–72.

**Disclaimer/Publisher’s Note:** The statements, opinions and data contained in all publications are solely those of the individual author(s) and contributor(s) and not of MDPI and/or the editor(s). MDPI and/or the editor(s) disclaim responsibility for any injury to people or property resulting from any ideas, methods, instructions or products referred to in the content.